Estimation of ship emission rates at a major shipping lane by long path DOAS measurements

Kai Krause[1], Folkard Wittrock[1], Andreas Richter[1], Stefan Schmitt[3, 4], Denis Pöhler[3, 4], Andreas Weigelt[2], and John P. Burrows[1]

[1]Institute of Environmental Physics, University of Bremen, Germany
[2]Federal Maritime and Hydrographic Agency (BSH), Hamburg, Germany
[3]Institute of Environmental Physics, University of Heidelberg, Germany
[4]Airyx GmbH, Heidelberg, Germany

Correspondence: Kai Krause (kakrau@iup.physik.uni-bremen.de)

Abstract. Ships are an important source of SO_2 and NO_x, which are key parameters of air quality. Monitoring of ship emissions is usually carried out using in situ instruments on land, which depend on favourable wind conditions to transport the emitted substances to the measurement site. Remote sensing techniques such as long path DOAS (LP-DOAS) measurements can supplement those measurements, especially in unfavourable meteorological conditions. In this study one year of LP-DOAS measurements made across the river Elbe close to Hamburg (Germany) have been evaluated. Peaks (i.e. elevated concentrations) in the NO_2 and SO_2 time series were assigned to passing ships and a method to derive emission rates of SO_2, NO_2 and NO_x from those measurements using a Gaussian plume model is presented. 7402 individual ship passages have been monitored and their respective NO_x, SO_2 and NO_2 emission rates have been derived. The emission rates, coupled with the knowledge of the ship type, ship size and ship speed have been analysed. Emission rates are compared to emission factors from previous studies and show good agreement. In contrast to emission factors (in gram per kilogram fuel) the derived emission rates (in gram per second) do not need further knowledge about the fuel consumption of the ship. To our knowledge this is the first time emission rates of air pollutants from individual ships have been derived from LP-DOAS measurements.

1 Introduction

Shipping plays an important role in the transport of goods around the world, with 80 - 90 % of world trade being carried by ships. Although shipping is an efficient way of transport, the total number of ships and the relatively high emission factors of air pollutants of ship engines, have an impact on the environment and human health (Alföldy et al., 2013). The contribution of ship emissions to the global emissions of NO_x and SO_2 was estimated to be about 15 % and 4-9 %, respectively (Eyring et al., 2010). NO_x emissions are high because of the design of the engines, which operate at high temperatures and pressures (Balzani Lööv et al., 2014). SO_2 emissions are high because of the high fuel sulphur content of the typically used shipping fuel (Balzani Lööv et al., 2014). NO_x and SO_2 emissions are nowadays limited by the International Maritime Organization (IMO) Marpol, Annex VI protocol, which sets global limits for fuel sulphur content and NO_x engine power-weighted emission rate. Further-more, emission control areas (ECAs) have been established in some regions, enforcing more strict emission rules.

For example the Baltic Sea, the North Sea, the English Channel and the coasts of the US and Canada are designated as ECA (emission control area) (Beecken et al., 2014). Most of the emissions caused by international shipping take place within 400 km of land and therefore have an impact on coastal air quality (Eyring, 2005). Due to the importance of ship emissions, a large number of studies has been performed previously. Measurements of air pollution, and consequently shipping emissions, are often performed with in situ instruments (e.g. Moldanová et al. (2009), Alföldy et al. (2013), Diesch et al. (2013), Beecken et al. (2014), Pirjola et al. (2014), Beecken et al. (2015), Kattner et al. (2015), Kattner (2019)), but remote sensing techniques such as differential optical absorption spectroscopy (DOAS) have also been successfully applied (e.g. Berg et al. (2012), Seyler et al. (2017), Seyler et al. (2019), Cheng et al. (2019)). Additionally, the impact of shipping emissions has been investigated by modelling studies (e.g. Eyring (2005), Ramacher et al. (2018), Ramacher et al. (2020), Tang et al. (2020)). In order to model the influence of ship emissions on air quality, one needs to characterize the international shipping fleet and to prescribe the emission behaviour of individual vessels. The information needed for this usually comes from in situ measurements, either on-board the ship or onshore. In both cases the statistics are limited, on-board measurements being restricted to a small number of ships, and onshore measurements depending on favourable wind conditions, to transport the emitted substances to the measurement site. Remote sensing techniques such as long path DOAS (LP-)DOAS can help to supplement in situ measurements, as the technique enables ship plumes, containing pollutants to be measured independent of meteorological conditions.

In this study, an approach to determine absolute emission rates of NO_x, NO_2 and SO_2 from LP-DOAS measurements is presented. The derived emission rates provide insight into the emission behaviour of the ship fleet entering the harbour of Hamburg, Germany, which is one of the largest ports in Europe.

2 Measurements and methods

2.1 Measurement site

Measurements made in this study were carried out in Wedel, a small town close to Hamburg, which is located on the river banks of the river Elbe. The river serves as the entrance route to the port of Hamburg and is well frequented by different types of ships going from or to Hamburg through the North Sea or the Kiel Canal. Most ships are container vessels, tankers, bulk carriers or reefer vessels. The measurement site is located on the northern banks of the river Elbe on the premises of the Waterways and Shipping Office (WSA) (53.570° N, 9.69° E) and is operated by the Federal Maritime and Hydrographic Agency (BSH) to monitor shipping emissions compliance according to MARPOL Annex VI. The standard instrumentation consists of in situ instruments to measure concentrations of SO_2, CO_2, NO_x and O_3. Those measurements are supplemented by an AIS (automatic identification system) receiver to obtain information about the passing ships, as well as meteorological measurements. All instruments are located close to the main shipping lane with a line of sight distance to the ships steaming from or to the port of Hamburg of 300 to 500 m. The port of Hamburg is located 10 km upriver from the measurement site and the ships still or already use their main engine. The prevailing wind directions in the area, which are from the south, are such that the emissions from shipping are often blown towards the measurement site. The southern river bank is rural and sparsely

Table 1. Characteristics of the LP-DOAS system.

Component	Details
Light source	Laser-Driven light source Energetiq EQ99
Optical fibres	200 μm, 800 μm
Telescope mirror	Diameter 0.3 m, focal length 1.5 m
Spectrometer	Acton Spectra Pro 300i
CCD	2048×512 pixel Roper scientific back-illum.
Measured wavelengths	280 – 362 nm, 0.53 nm resolution

55 populated without large sources of air pollution. A detailed description of the in situ instruments used on site can be found in Kattner et al. (2015) who used these data to derive fuel sulphur content for passing ships.

2.2 LP-DOAS instrument

To monitor shipping emissions by optical remote sensing, a LP-DOAS instrument was set up on the northern river bank in April 2018. The instrument uses an artificial light source to emit a beam of light across the river, which is reflected by an array
60 of retro reflectors that is mounted onto a lighthouse on the southern river bank at an altitude of approximately 35 m above ground level. The distance between emitting telescope and retro reflector array is 2.87 km, leading to a total light path of 5.74 km. The reflected light beam is then measured and evaluated using the DOAS technique, which is explained in the next section. The technical details of the instrument are summarized in Table 1. The measurement geometry across the river is shown in Figure 1.
65 The instruments measurement cycle consists of one reference lamp spectrum followed by four blocks of 32 atmospheric spectra. After each block an atmospheric background spectrum is measured. Each spectrum consists of ten individual scans, which are co-added. The exposure time of these individual scans is tied to a fixed saturation of the CCD, with a maximum exposure time of 0.3 seconds. This results in a temporal resolution of 3 seconds.

2.3 Differential Optical Absorption Spectroscopy (DOAS)

70 The basic principle of spectroscopic measurements is given by Lambert-Beer's law which describes the absorption of electro-magnetic radiation by matter:

$$I(\lambda) = I_0(\lambda) \cdot exp(-\sigma(\lambda) \cdot c \cdot L), \tag{1}$$

where $I_0(\lambda)$ is the initial intensity, $I(\lambda)$ is the intensity after passing through a medium of a given thickness L containing the absorbing species in concentration c and $\sigma(\lambda)$ is the absorption cross-section at a given wavelength λ. In DOAS the
75 absorption cross-section is separated into two parts, the first one describing broadband absorption and elastic scattering can be
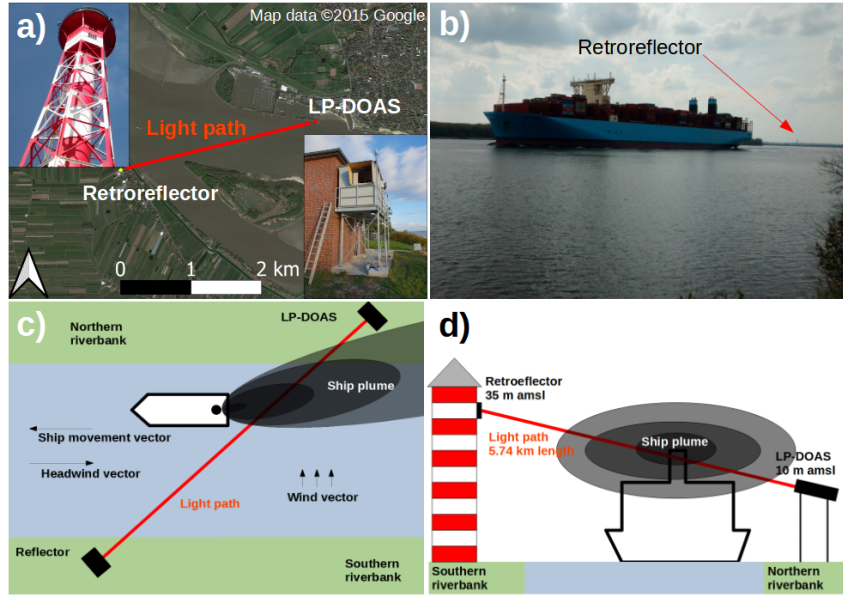
Figure 1. a) Satellite image of instrument location, with LP-DOAS marked as a red dot on the northern river bank and retro reflector position marked as yellow dot on the southern river bank. b) Image of a passing container ship next to the measurement site. c) Schematic overview of the measurement geometry of the LP-DOAS for a passing ship leaving Hamburg towards the North Sea, seen from above. d) same as c) but seen from the port of Hamburg. Note that c) and d) are not to scale.

approximated by a polynomial, while the second part (σ'), called differential cross-section, contains the narrow-band absorption structures. In the presence of N absorbing species, each of them has to be included with their respective absorption cross-section. Taking this into account, the DOAS equation results:

$$\ln \frac{I_0(\lambda)}{I(\lambda)} = \sum_{i=1}^{N} L \cdot c_i \cdot \sigma_i' - \sum_{p} \cdot a_p \cdot \lambda^p. \tag{2}$$

80   A polynomial and the differential cross sections of all relevant absorbing species are then fitted to the measured optical depth $\ln \frac{I_0(\lambda)}{I(\lambda)}$, resulting in the coefficients of the polynomial a_p and the integrated number densities of the respective absorbers along the light path $L \cdot c_i$. From this quantity, the concentration can be determined because L is known from the experiment set-up, c_i being the mean concentration of species i along L.

2.4 Data analysis

85   In order to derive the contribution of an individual ship to the total measured integrated concentration of a pollutant, further steps are needed. The data analysis comprises three steps. Firstly the measured spectra were analysed using the DOAS tech-

Table 2. DOAS fit settings for the retrieval of SO_2, NO_2 and O_3.

Trace gas	SO_2	NO_2	O_3
Fit window	297.0 - 309.0 nm	334.5 - 356.5 nm	282.0 - 314.5 nm
Polynomial degree	3	3	3
Cross sections	NO_2 298 K (Vandaele et al., 1996)	NO_2 298 K (Vandaele et al., 1996)	NO_2 298 K (Vandaele et al., 1996)
	O_3 293 K (Serdyuchenko et al., 2014)	O_3 293 K (Serdyuchenko et al., 2014)	O_3 293 K (Serdyuchenko et al., 2014)
	SO_2 294 K (Vandaele et al., 1996)	O_4 293 K (Thalman and Volkamer, 2013)	SO_2 294 K (Vandaele et al., 1996)
	HCHO 297 K (Meller and Moortgat, 2000)	HCHO 297 K (Meller and Moortgat, 2000)	HCHO 297 K (Meller and Moortgat, 2000)
		HONO 296 K (Stutz et al., 2000)	

nique to determine the concentration of the absorbing gas along the path of the electromagnetic radiation. Secondly the elevated concentrations which we attribute to a particular passing ship are estimated. Thirdly the emission rate of the trace gas for the assigned ship is calculated.

90   The fit settings to retrieve NO_2, SO_2 and O_3 time series from the measured spectra are shown in Table 2.

An example time series of the fitted trace gases is shown in Figure 2. The blue lines show the fitted trace gas time series and the orange lines the corresponding detection limit. The gray dashed lines mark passing ships that have been assigned to a peak. The green lines shows the estimated background concentration. Following Stutz and Platt (1996), the DOAS measurement error was defined as two times the DOAS fit error and the detection limit for the trace gases was defined as two times the

95   measurement error (four times the DOAS fit error), which results in a median detection limit of 190 pptv for NO_2, 59 pptv for SO_2 and 253 pptv for O_3. Before further analysis DOAS fits with a RMS higher than 0.01 are removed from the dataset. These high RMS usually occur when a ship blocks the light path.

Comparison of the concentrations of the in situ measurements and the DOAS measurements is not straight forward, as both systems measure different air masses. The in situ measurements rely on the transport of air masses to the measurement site,

100   whereas the LP-DOAS measures the integrated number density of the respective absorbers along the light path. As only a small portion of the light path is affected by a plume, the LP-DOAS measures a lot of background concentration and possible enhancements of NO_2 or SO_2 are lower than for the in situ instruments. Nevertheless both measurement systems show similar results (e.g. Figure 3).
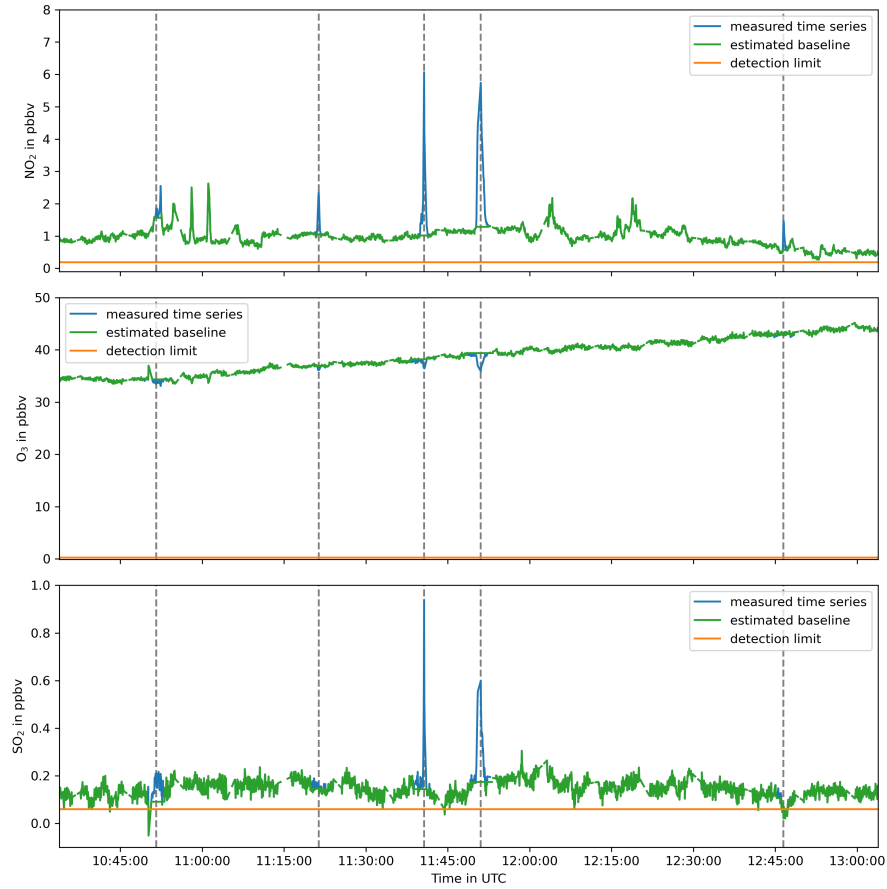
Figure 2. Example time series of the fitted trace gases from 19th August 2018 between 10:30 and 13:00 UTC. In each plot the blue line shows the fitted time series of the respective trace gas and the orange line shows the respective median detection limit. The grey dashed lines mark passing ships, that have been assigned to a peak in the time series. The green line shows the calculated background.

2.4.1 Peak identification

105 For each emission plume, measured maxima, i.e. enhanced amounts of NO_2, SO_2 and a minimum, i.e. a diminished amount of O_3 values are found, as expected. To identify such peaks, a low pass filtered time series is calculated using a running median with a window size of five minutes. The low pass filtered time series represents the background concentration including influences by meteorological factors but excludes the short term variations caused by plumes of passing ships. The low pass filtered time series is then subtracted from the original time series, resulting in a time series which is close to zero on average, 110 but contains several peaks. If one of those peaks exceeds a predefined threshold, then the peak is marked as a valid increase in trace gas concentration caused by some sort of emission, e.g. a passing ship. In this study the threshold was set to four times
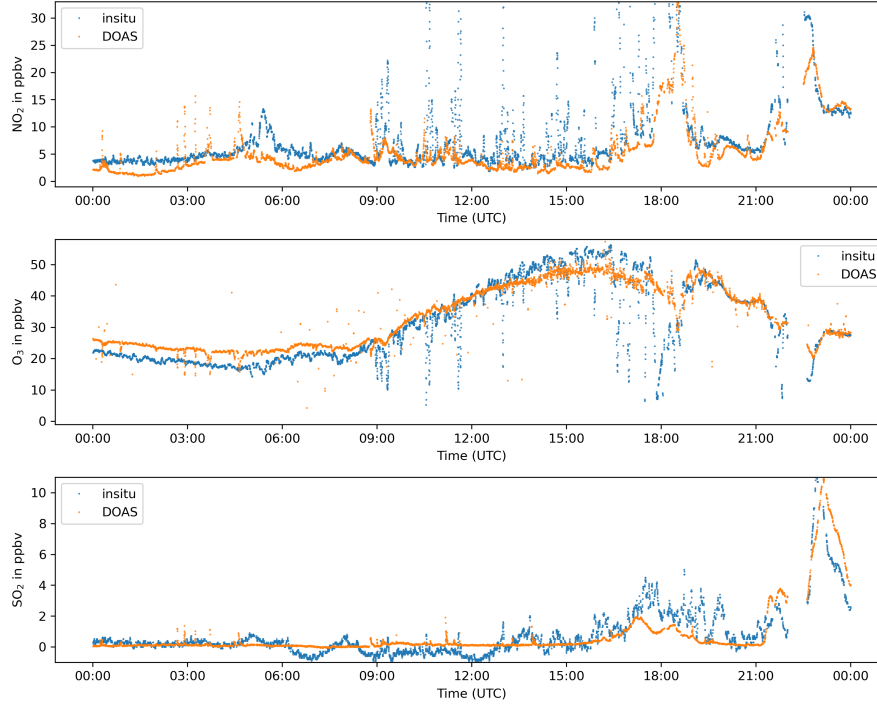
Figure 3. Time series of NO$_2$, O$_3$ and SO$_2$ measured by the in situ instruments (blue) and the LP-DOAS (orange) on 20th July 2018.

the DOAS fit error of the respective trace gas measurement. This analysis is carried out separately for each relevant trace gas (NO$_2$, SO$_2$, and O$_3$).

In the next step, the identified peaks are assigned to individual ships. The assignment is based on AIS data of passing ships. AIS data contains the current position, speed and heading of the ship, as well as other, more general information about the ship itself (e.g. speed, course, type, length, destination, ...). The AIS data is transmitted in regular intervals of two to thirty seconds and is interpolated to one second time resolution using linear interpolation between two received AIS messages. For each detected peak in the trace gas time series it is then checked, if there was a ship in a position that could have caused the increase in trace gas concentration. If there is a single ship in a position that could be the source of the enhancement of the trace gas concentration, this ship is assigned to the respective peak. The assignment is based on position and time. For each peak occurrence t_{peak}, a time window of $(t_{peak} - \Delta t_{before}) < (t_{peak} + \Delta t_{after} + \Delta t_{dyn})$ is defined, where Δt_{before} is set to 30 and Δt_{after} is set to 120 seconds, and Δt_{dyn} is calculated as the length of the ship divided by the speed of the ship. The window starts before peak occurrence to accommodate for ship plumes that are transported by wind through the light path before the ship itself passes the light path. The windows are extended dynamically by ship size and ship speed to incorporate that larger ships may need a longer time to pass through the light path. Due to the length of the defined time window, several AIS positions of an individual ship are possible source positions. The final assignment is based on distance to the light path as well as course and length of the ship. The first position where the ship could have fully passed the light path is assigned as the ship position

responsible for the trace gas peak. In median the time difference between measurement of the peak maximum and the assigned AIS signal is 20 seconds. The approach fails if the traffic density of ships is too high, making the unambiguous attribution of a plume to a particular ship impossible. Evaluation of the AIS data shows that on average there are 110 ship passages per day.

Neglecting the additional criterion of a full pass and using stricter time windows around each peak, a higher number of peaks could be attributed to ships, but this also increases the chance of mismatches and the assignment of mixed plumes of several ships to a single ship.

2.4.2 Estimation of NO_x from measured NO_2

Being restricted to the wavelength range between 280 and 360 nm, the LP-DOAS measures NO_2, while the ship emits nitrogen oxides (NO_x) as NO and NO_2. A part of the NO_2 is produced during the combustion process and emitted by the ship directly, while another part is formed after emission by reaction with ozone in the atmosphere:

$$NO + O_3 \rightarrow NO_2 + O_2. \tag{R1}$$

To estimate the total NO_x emission, a simple approach is used to convert the measured NO_2 concentrations to NO_x concentrations. The correct NO_2/NO_x ratio can be obtained by summing the NO_2 and O_3 signals and plotting this sum against the measured NO_x concentration (Clapp, 2001; Kurtenbach et al., 2016). This kind of analysis has been carried out using data from the in situ measurements which provide NO_x, NO_2 and O_3 observations and results in a mean NO_2/NO_x ratio of 0.138 (see Figure 4) which agrees with previous studies Cooper (2001). This means most of the emitted NO_x is emitted as NO and only a smaller fraction is directly emitted as NO_2. The NO_2 peak observed by LP-DOAS can then be converted to NO_x using the following formula:

$$NO_x = \frac{(\Delta NO_2 + \Delta O_3)}{NO_2/NO_x ratio} \tag{3}$$

where ΔNO_2 is the increase in NO_2 caused by the ship and ΔO_3 is the decrease in O_3 caused by the reaction of emitted NO with atmospheric O_3 and is also measured by the LP-DOAS. Using this approach, the total amount of measured NO_2 is corrected for the NO_2 that formed during transport in the atmosphere, and the remaining NO_2 is the amount primarily emitted by the ship. This primarily emitted NO_2 is then used to estimate the amount of emitted NO_x using again the NO_2/NO_x ratio. This procedure assumes that the NO_2/NO_x ratio is the same for all ships and that no other species are emitted which could impact on the NO_2 production or ozone removal. Based on the compact correlation found (see Figure 4), these assumptions appear to be justified. There is no indication for further dependencies of the NO_2/NO_x ratio on the position of the source ship, the wind direction or the age of the plume.
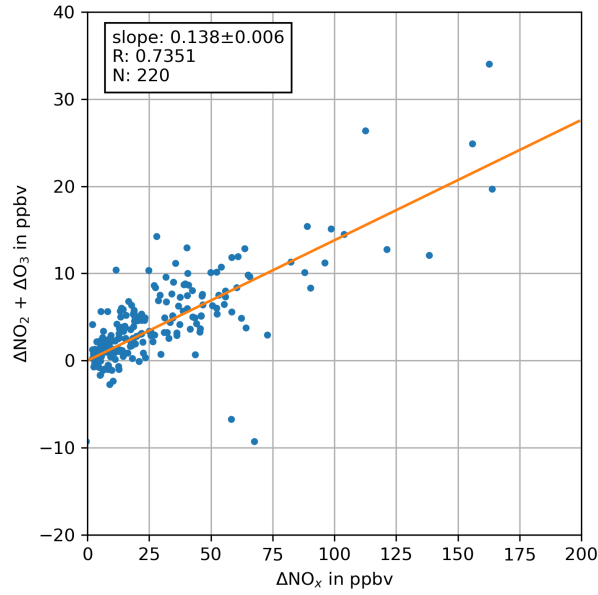
Figure 4. Plot of $\Delta NO_2 + \Delta O_3$ against ΔNO_x from peaks measured with the in situ instruments between April 2018 and May 2019. All concentrations have been corrected for background concentrations. For this analysis, 220 manually quality checked peaks were used. This results in a slope (a NO_2/NO_x ratio) of 0.138 with a respective standard error of 0.006.

2.4.3 Estimation of emission rate

As the LP-DOAS instrument does not measure the concentration of the trace gases at the stack, a model has to be applied to estimate the emission from the concentration enhancement found for a given light path. This conversion is based on the assumption that the plume of a single ship can be described by a simple Gaussian plume model (Pasquill, 1968) and can be expressed mathematically by Eq. 4:

$$C(x,y,z) = \frac{Q}{2\pi U \sigma_y \sigma_z} \cdot \exp(\frac{-y^2}{2\sigma_y^2}) \cdot [exp(\frac{-(z-H)^2}{2\sigma_z^2}) + exp(\frac{-(z+H)^2}{2\sigma_z^2})] \tag{4}$$

where Q is the emission rate of a substance in gram per second, U is the wind speed in meter per second along the main wind direction (aligned with x), σ_y and σ_z are the dispersion parameters in horizontal (y) and vertical (z) direction in meter and H is the height of the plume center in meter. The dispersion parameters depend on x, the atmospheric stability and the surrounding environment, which differs for open country and urban conditions. A simple classification scheme for the stability classes is shown in Table 3, while the corresponding dispersion parameters are listed in Table 4.

To determine atmospheric stability at the measurement site the wind speed measurements of the in situ instruments are used, while incoming global radiation and cloud coverage are taken from a nearby measurement station of the German Weather Service located at the Hamburg-Airport (DWD Climate Data Center (a), DWD Climate Data Center (b)).

Table 3. Atmospheric stability classification scheme based on surface wind speed and solar insulation for day time conditions and cloud cover during night time conditions (Pasquill, 1968). Ranging from very unstable (A) to moderately stable (E).

Surface wind speed 10 m a.g.l. ($\mathrm{m\,s^{-1}}$)	Daytime solar radiation			Night time cloud cover	
	Strong	Moderate	Slight	>= 4/8 clouds	<= 3/8 clouds
< 2	A	A - B	B	-	-
2-3	A - B	B	C	E	F
3-4	B	B - C	C	D	E
4-6	C	C - D	D	D	D
> 6	C	D	D	D	D

Table 4. Atmospheric dispersion parameters σ_y and σ_z for different stability classes in dependence of distance (x) from source in meter. For intermediate cases such as A - B the average of both values has been taken (Briggs, 1973).

Stability class	$\sigma_y(x)$	$\sigma_z(x)$
A	$0.22x(1+0.0001x)^{-0.5}$	$0.20x$
B	$0.16x(1+0.0001x)^{-0.5}$	$0.12x$
C	$0.11x(1+0.0001x)^{-0.5}$	$0.08x(1+0.0002x)^{-0.5}$
D	$0.08x(1+0.0001x)^{-0.5}$	$0.06x(1+0.0015x)^{-0.5}$
E	$0.06x(1+0.0001x)^{-0.5}$	$0.03x(1+0.0003x)^{-0.5}$
F	$0.04x(1+0.0001x)^{-0.5}$	$0.016x(1+0.0003x)^{-0.5}$

In order to calculate the emission rate of a ship, the model is evaluated once with an arbitrary emission rate (Q_{model}), using the ship's position as the starting point of the plume. The effective height of the plume center is set to the height of the funnel above water level assuming that the plume quickly bends down due to wind and the movement of the ship. As the height of the ship stack is not transmitted in the AIS, the height of the stack is estimated from pictures of the respective ship, preferably taken by the camera of one of the instruments, otherwise pictures from marinetraffic.com were used (MarineTraffic). Dispersion parameters σ_y, σ_z are chosen according to atmospheric stability. To account for the movement of the ship, the wind speed and direction have been combined with the ship movement to an apparent wind speed and apparent wind direction (Berg et al., 2012):

$$U_{aw} = \sqrt{(v_{wind\,N} + v_{ship\,N})^2 + (v_{wind\,E} + v_{ship\,E})^2} \tag{5}$$

$$\theta_{aw} = -\mathrm{atan2}[(v_{wind\,E} + v_{ship\,E}), (v_{wind\,N} + v_{ship\,N})] \tag{6}$$

where $v_{wind\,E}$, $v_{ship\,E}$ and $v_{wind\,N}$, $v_{ship\,N}$ are the eastern and northern velocity components of the wind vector and ship movement vector, respectively. Equation 6 uses the commonly available atan2 variation of the arctangent function which returns the inverse tangent of the first and second argument to the function (Berg et al., 2012).

As the real emission rate at the ships chimney (Q_{meas}) is unknown, this model run only gives insight into the dispersion of the emitted species. In order to retrieve the desired emission rate for a certain species emitted by the ship, the concentration measured at the measurement site (C_{meas}) is compared to the modelled concentration (C_{model}) along the light path, where C_{meas} is the already background corrected measured trace gas concentration. The correction is applied to each peak individually and is carried out by subtracting the mean concentration 30 seconds before and after the peak from the peak itself. The low-pass filtered time series used to identify the peaks is not used as a background, as it may overestimate the background concentration in cases of high traffic density. As the LP-DOAS measurement is integrating along the light path C_{model} is obtained by averaging all model grid cells along a path through the model grid, which corresponds to the light path during the measurement (see Figure 1). The LP-DOAS instrument measures not only the pure emission of the start point, but also older parts of the plume at the same time. The modelled region covers an area of approximately 2800 m x 700 m and the assigned ship position is always very close to the light path. Therefore the slightly different time of emission is neglected for simplicity and it is assumed that the measured plume is the result of the pure emission at the start point. As the time between emission and measurement by the LP-DOAS is on the order of seconds, possible effects of NO_2 photolysis are small and are neglected. Assuming all parameters are estimated correctly, the only difference between modelled concentration and measured concentration is caused by a different emission rate. Therefore Q_{meas} can be estimated by the following equation:

$$Q_{meas} = \frac{C_{meas}}{C_{model}} \cdot Q_{model} \tag{7}$$

This approach assumes that the motion vector of the ship and the emission rate is constant for the time between emission and measurement of the enhanced concentration.

2.4.4 Estimation of uncertainty

The uncertainty of the emission rate is given by:

$$\sigma_Q = \sqrt{\left(\frac{\partial Q_{meas}}{\partial C_{meas}} \cdot \sigma_{C\,meas}\right)^2 + \left(\frac{\partial Q_{meas}}{\partial C_{model}} \cdot \sigma_{C\,model}\right)^2} \tag{8}$$

where $\sigma_{C\,meas}$ is the uncertainty of the measured trace gas concentration and $\sigma_{C\,model}$ the uncertainty of the modelled trace gas concentration. In case of NO_x, $\sigma_{C\,meas}$ consists of the uncertainty of the NO_2 concentration, the uncertainty of O_3 and the uncertainty of the NO_2/NO_x ratio.

To calculate $\sigma_{C\,model}$, Monte-Carlo-Simulations are performed for each individual passing ship, where U_{aw}, θ_{aw}, atmospheric stability, latitudinal- and longitudinal position of the ship and the funnel height of the ship are varied within their

respective uncertainty range. The assumed uncertainty for each parameter is shown in Table 5. This results in a set of simulations for every input parameter, and for each simulation in the respective set, the concentration along the artificial light path is determined. A set for a single input parameter (j) is then summarized as mean concentration ($mean_{Cj}$), the respective standard deviation (σ_{Cj}), minimum (min_{Cj}) and maximum value (max_{Cj}). The model uncertainty is then calculated as:

$$\sigma_{C\,model} = \sqrt{\sigma_{C\,U\,aw}^2 + \sigma_{C\,\theta\,aw}^2 + \sigma_{C\,stability}^2 + \sigma_{C\,lon}^2 + \sigma_{C\,lat}^2 + \sigma_{C\,H}^2} \tag{9}$$

where each σ_{Cj} is the standard deviation of the modelled trace gas concentrations of the Monte-Carlo-Simulations with respect to changes of an individual parameter j. As the parameters are changed individually, possible interactions between changes of more than one parameter at a time are neglected.

The largest error source is the uncertainty of the position of the emission source, as it has a large impact on which part of the plume is assumed to be measured, and thus has a large impact on the derived C_{model}. The position is determined by the data transmitted by the AIS with an average error of 10 m or less. However, since the the location of the funnel in relation to the AIS transmitter on the ship itself is not known, the positional error also depends on the dimensions and orientation of the ship. For the calculation it is assumed that the emission source is located at the position given by the AIS. It is assumed that the transmitter is located at or close to the bridge of the ship, and that the funnel is also close to it. For smaller ships this is certainly true, due to the small dimensions of the ship. For larger ships such as tankers and container ships, different designs exist. It is assumed that the transmitter is close to the bridge here as well, and that the main exhaust is not further away from that position than half the ship width or length.

Additionally the height of the emission depends on the stack height and the water level. The stack height is estimated from pictures of the ship which gives an initial uncertainty of the value, furthermore the height above water level depends on the draft of the ship, which is transmitted by the AIS. At the measurement site the water level of the river Elbe is not only influenced by the amount of water flowing downstream but also by the tide. The water level is assumed to be between the long-term mean high and mean long-term low water level.

The second largest source of errors is the apparent wind used in the calculation. The apparent wind itself is calculated from the horizontal wind velocity vector and the ship velocity vector. In most cases, the magnitude of the ship velocity vector is large compared to the wind velocity vector, and therefore the uncertainty is dominated by the uncertainty of the ship's speed and course. The smallest error source is the uncertainty of the derived trace gas time series.

For NO_x, the uncertainty of the derived NO_2/NO_x ratio is another important factor for the overall uncertainty of the derived emission rate. As the NO_2/NO_x ratio is in the denominator of equation 3, even a small uncertainty of the ratio can lead to significant changes in the estimated NO_x concentration. Generally it is assumed the NO_2/NO_x ratio is the same for all ships, which is also supported by the compact correlation found in Figure 4, but the ship type and operation mode of the engine can also have an influence on this ratio.

Table 5. Uncertainties of the input parameters used in the Monte-Carlo-Simulations.

Abbreviation	Name	Calculation of value
σ_{lon}	ship extent in longitudinal direction	$\frac{1}{2} \cdot (|length \cdot \sin(heading)| + |width \cdot \cos(heading)|)$
σ_{lat}	ship extent in latitudinal direction	$\frac{1}{2} \cdot (|length \cdot \cos(heading)| + |width \cdot \sin(heading)|)$
σ_H	plume height	$\sqrt{\sigma_{fh}^2 + \sigma_{wl}^2}$
σ_{fh}	funnel height	estimated: 5 m
σ_{wl}	water level	mean high water level - mean low water level
σ_{aw}	apparent wind speed	$\sqrt{\sigma_{v_{wind\,N}}^2 + \sigma_{v_{ship\,N}}^2 + \sigma_{v_{wind\,E}}^2 + \sigma_{v_{ship\,E}}^2}$
$\sigma_{v_{wind\,N}}$	wind speed	standard deviation of northern wind component
$\sigma_{v_{wind\,E}}$	wind speed	standard deviation of eastern wind component
$\sigma_{v_{ship\,N}}$	ship speed	estimation based on $0.514 \, \mathrm{m\,s^{-1}}$ uncertainty in speed
$\sigma_{v_{ship\,E}}$	ship speed	and 10 ° uncertainty in heading
$\sigma_{\theta_{aw}}$	apparent wind direction	estimated: 10 °
$\sigma_{stability}$	stability	atmospheric dispersion parameters of class with lower stability and higher stability than the assigned class
σ_{NO_2/NO_x}	NO$_2$/NO$_x$ ratio	standard error of the slope (0.006)
$\sigma_{c_{meas}}$	DOAS measurement error	individual DOAS measurement error for each trace gas
		mean value for NO$_2$ 1.5 %
		mean value for SO$_2$ 17.7 %
		mean value for O$_3$ < 0.1 %

3 Results

240 Between April 2018 and May 2019 a total number of 7402 passing ships were identified and assigned to a peak in the trace gas time series. Due to technical problems with the instrument, there were only 233 days of measurements during this time period. Most of the measurements took place between June 2018 and February 2019, while before and after there were only individual days of measurements.

For each ship passage, emission rates of SO$_2$, NO$_2$ and NO$_x$ were calculated. This dataset has then been filtered to remove 245 non-physical results such as very high emission rates of several tons per second. These non-physical values occur when the assumptions within the Gaussian plume model do not reflect the situation during the measurement and therefore the shape of the calculated plume does not match the real plume.

To eliminate such cases before further investigation, three criteria have been defined. If one of these criteria is violated for a single input parameter j for a given individual measurement, the derived emission rate is omitted from the further analysis. 250 The criteria are:

1) $mean_{C\,j}/C_{model}$ has to be between 0.8 and 1.2, to eliminate cases where the uncertainty introduced by the input parameter systematically leads to too high or low derived concentrations.

2) σ_{Cj}/C_{model} has to be lower than 0.4, to eliminate cases that have a high variability if input parameters are varied within their uncertainties.

255   3) The difference between max_{Cj}/C_{model} and min_{Cj}/C_{model} has to be smaller than 1, to eliminate cases with a large spread between minimum and maximum value.

After this quality check a total of 886 NO_x, 1069 SO_2 and 1375 NO_2 emission rates were left for further analysis, and the emission rates have an uncertainty of 43 % in the mean and 35 % in median. The exclusion of many measured ships is a result of the here applied plume model and not due to the LP-DOAS measurement itself. It is part of the current developments to

260   increase the output rate with different measurement configurations. The total number of ships differs because the assignment of a ship to a peak in the trace gas time series is carried out for each trace gas individually, which leads to some differences between SO_2 and NO_2 signal strength. The sulphur content of shipping fuel is limited to 0.10 % S M/M for seagoing and 1×10^{-5} % S M/M for inland ships, resulting in ship passes which clearly cause a peak in NO_2 while the enhancement in SO_2 is too low to be detected as a peak. For NO_x the concentrations of ΔNO_2 and ΔO_3 are summed and under circumstances with

265   a high temporal variability within those trace gas concentrations, the background correction for the individual peaks might be erroneous and thus the sum can be zero or even negative. In such cases the NO_x emission rate is not calculated. As an example, Figure 5 shows the difference between the unfiltered and filtered dataset for NO_x emission rates for different ship length classes as box plots.

The unfiltered data set shows a large variability, indicated by the large boxes, while the filtered data set clearly shows a lower

270   variability and a narrow distribution around the median of the respective length class. An exception is the 150 m length class, which still shows a high variability. This variability is caused by dredging ships and will be discussed in more detail in one of the next paragraphs.

There are several ships which passed the measurement site multiple times or even on a regular basis. This allows to determine the emission rate for a single ship under different measurement conditions. Emission rates of SO_2 and NO_x for a variety of

275   ships are shown in Figure 6 as box plots. Generally the 25% and 75% percentiles are close to their respective median values, which indicates that the estimation method works consistently. A larger variability of the emission rate for an individual ship usually indicates special operating conditions of the ship. Examples for this are the two dredging ships. These ships can operate under varying conditions and do not necessarily only pass by, but sometimes excavate material from the bottom of the river. This might lead to higher engine loads in general or the usage of additional auxiliary engines, which in turn increases the total

280   emission of those ships. At other times, those ships just steam through the light path without carrying out additional work, which explains the low emission rates observed on some passes. A combination of these different operating conditions leads to the high spread seen in the box plots.

Differences in emission rates between ship types can be seen. Figure 7 shows box plots of the SO_2 and NO_x emission rates for inland ships, sea going ships and dredging ships. Generally sea going ships tend to have higher emission rates, with a

285   median of 5.23 ± 14.0 g s^{-1} for NO_x and 0.28 ± 0.87 g s^{-1} for SO_2, while for inland ships the median is 1.93 ± 8.17 g s^{-1} for NO_x and 0.06 ± 0.19 g s^{-1} for SO_2. The difference in SO_2 can be attributed to two different factors. First of all, inland ships use fuel having a lower fuel sulphur content, which automatically decreases the amount of SO_2 emitted per amount of
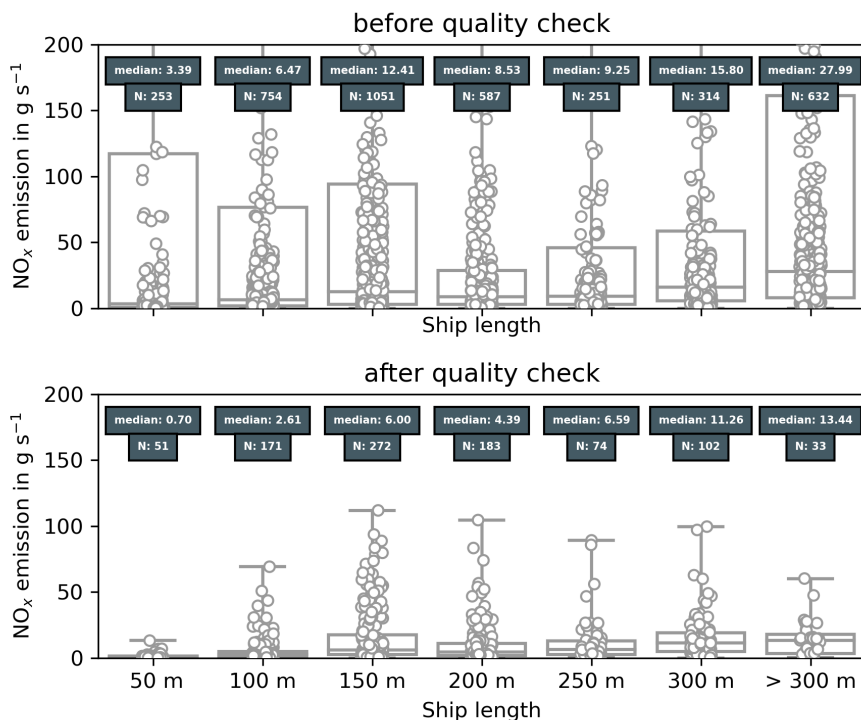
Figure 5. Box plot of NO_x emission rates in $g\,s^{-1}$ for different ship sizes. Boxes indicate the 25% and 75% percentile, the line in the middle is the median and the bars show minimum and maximum values. Dots show individual measurements. Dark grey boxes show the median emission rate and total number of observations for this length class.

fuel. Secondly, inland ships are smaller and have smaller engines, consuming less fuel per unit time. In combination these two factors explain the lower SO_2 emission rates found for inland ships. Most of the NO_x formed during combustion consists of atmospheric nitrogen and oxygen. The amount of NO_x formed is temperature dependent, higher engine temperatures leading to higher amounts of NO_x (Alföldy et al., 2013). For inland ships there is already a limit for their NO_x emissions, while for seagoing ships there was none at the time the measurements took place, which explains the higher NO_x emission rates for seagoing ships. This can also be seen in Figure 8, where the NO_x emission rate is categorized for different ship size classes and the median emission rate increases with size. The emission rates are also correlated to ship speed, faster ships generally having a higher emission rate (see Figure 9). The decrease in the SO_2 emission rate for ship speeds larger than $7\,m\,s^{-1}$ is probably caused by the low number of observations, which only include a single individual ship.

The determined median SO_2 emission rate for inland ships is larger than the expected SO_2 emissions by those ships. A simple calculation of the expected SO_2 emission rate can be made by multiplying the fuel sulphur content with the amount of fuel used per unit of time. Table 7 shows those calculations for inland diesel fuel and fuel which qualifies for the SECA limit of $0.10\,\%\,S\,M/M$. The observed median SO_2 emission rate for inland ships is $0.06\,g\,s^{-1}$, which is considerably higher than the
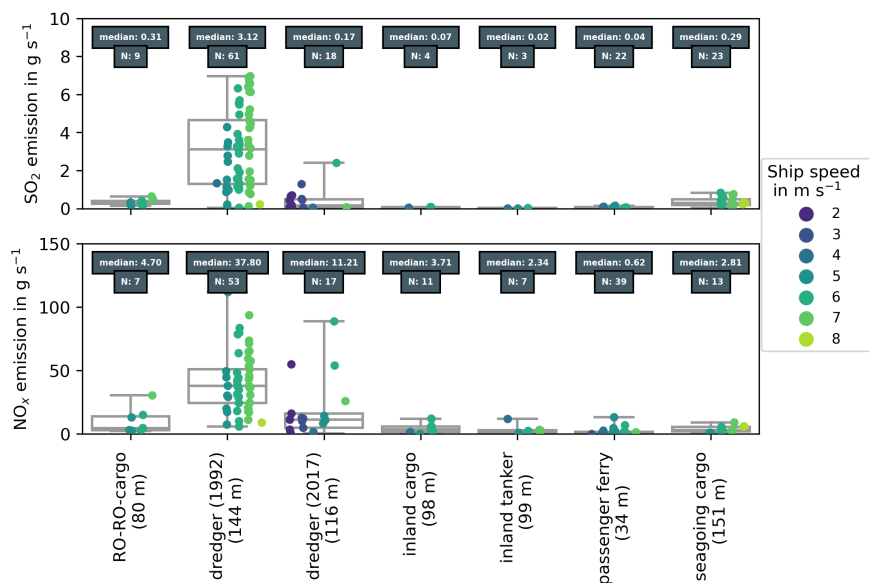
Figure 6. Box plot of SO_2 and NO_x emission rates in $g\,s^{-1}$ for individual ships, their respective length is given in brackets. Boxes indicate the 25% and 75% percentile, the line in the middle is the median and the bars show minimum and maximum values. Dots show individual measurements and are colour coded by corresponding ship speed. Dark grey boxes show the median emission rate and total number of observations for this ship.

expected SO_2 emission rate ($0.0009\,g\,s^{-1}$) for the typical fuel consumption of an inland ship and still too high when assuming the typical fuel consumption of a much larger ship.

But it has however to be kept in mind that the SO_2 emission rates, especially for inland ships, are biased towards high emitters, as some ships can only be identified in the NO_2 time series, while there is no detectable peak in the SO_2 time series. Ships with low SO_2 emissions are therefore underrepresented in the data set. In order to calculate a more representative mean SO_2 emission rate for inland ships, the total number of observed inland ships has to be taken from the NO_2 dataset instead, and all cases without an associated SO_2 emission rate are treated as zero SO_2 emission. The total number of observed inland ships would then be 296 (identified from the NO_2 peaks and with valid NO_2 emission rate) and 220 of them would be treated as zero SO_2 emitters. This results in a mean SO_2 emission rate of $0.03\,g\,s^{-1}$ with and median emission rate near zero, which means the SO_2 emissions for inland ships are often below the detection limit of the LP-DOAS instrument. For sea going ships the method works better and the median SO_2 emission rate ($0.28\,g\,s^{-1}$) lies in the range estimated in Table 7.

For 26 individual ship passages (excluding dredging ships), the derived SO_2 emission rates are above the upper limit estimated in Table 7, which possibly indicates that those ships use fuel which does not comply with the SECA limit of 0.10 % M/M.
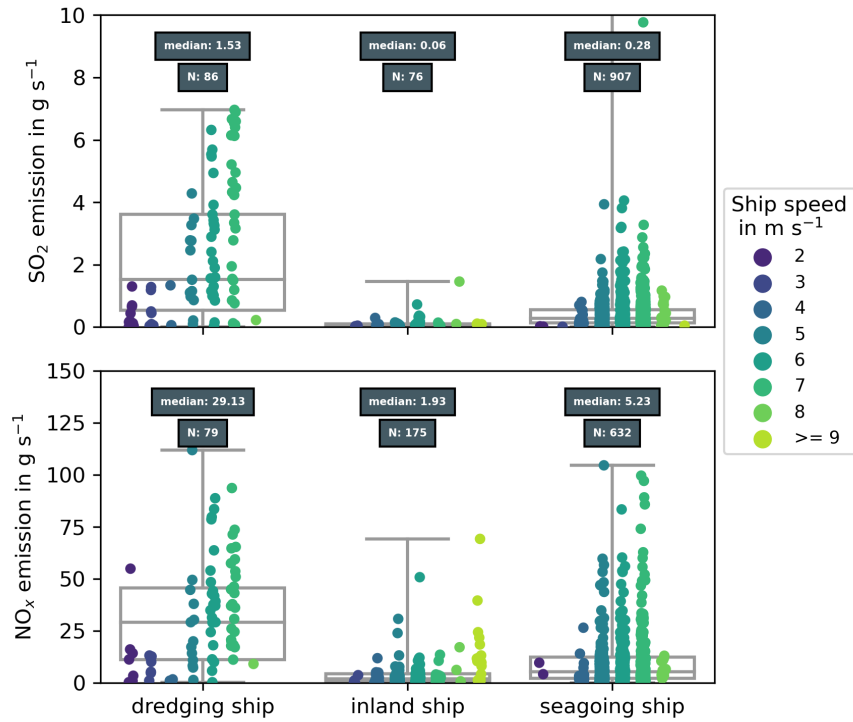
Figure 7. Box plot of SO_2 and NO_x emission rates in $\mathrm{g\,s^{-1}}$ for different ship types. Boxes indicate the 25% and 75% percentile, the line in the middle is the median and the bars show minimum and maximum values. Dots show individual measurements and are colour coded by corresponding ship speed. Dark grey boxes show the median emission rate and total number of observations for each ship type.

315   Most studies derive emission factors, which specify the mass of air pollutant released per mass of burnt fuel, whereas emission rates are less commonly reported. To compare these two physical quantities, further knowledge of fuel consumption is required. Table 6 shows the derived emission rates in comparison to the results of other studies under the assumption of two different fuel consumption scenarios. The lower value describes typical fuel consumption of an inland ship (about $165\,\mathrm{kg\,h^{-1}}$) and the upper value describes the fuel consumption of a large container ship, with carrying capacity of roughly 14.000 TEU,

320   at a speed of $7\,\mathrm{m\,s^{-1}}$ ($2000\,\mathrm{kg\,h^{-1}}$) (Notteboom and Vernimmen, 2009), which is slightly faster than the typical speed for the largest passing ships ($6\,\mathrm{m\,s^{-1}}$).

     In all cases the median emission rate derived by our method lies within the range estimated using the emission factors of other studies, although closer to the lower bound. This is reasonable, because most passing ships are seagoing ships, with higher fuel consumption than inland ships and at the same time do not belong to the largest ship class with the highest fuel

325   consumption.

     Comparison to emission rates of Berg et al. (2012) shows larger differences. Berg et al. (2012) found a mean emission rate of $11.4 \pm 7.8\,\mathrm{g\,s^{-1}}$ for NO_2 and $14.6 \pm 9.1\,\mathrm{g\,s^{-1}}$ for SO_2, while in this study the mean NO_2 emission rate is $1.5 \pm 2.9\,\mathrm{g\,s^{-1}}$
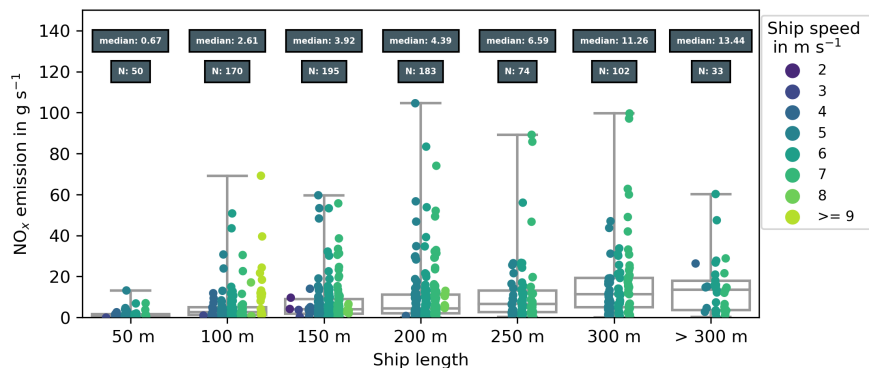
Figure 8. Box plot of NO_x emission rates in $g\,s^{-1}$ for different ship lengths. Boxes indicate the 25% and 75% percentile, the line in the middle is the median and the bars show minimum and maximum values. Dots show individual measurements and are colour coded to corresponding ship speed. Dark grey boxes show the median emission rate and total number of observations for this length class. Data of dredging ships has been excluded.

and the mean SO_2 emission rate is $0.6 \pm 1.1\ g\,s^{-1}$. This can be explained by different reasons. First of all Berg et al. (2012) observed transects of ship plume on the open seas, where the fuel sulphur limit at the time was $1.0\ \%\ M/M$, which is a factor

330   of 10 higher than at the time of the measurements in this study, thus the emission rates of SO_2 should also be higher by roughly a factor of ten. Additionally ships on the open seas travel at higher speeds than at our measurement site, which increases their fuel consumption and thus their SO_2 emission rates. Considering the different fuel sulphur content and different speeds, both mean emission rates agree within their respective uncertainties.

      The difference in the NO_2 emission rates might be also caused by the age of the observed plume, because in older plumes

335   emitted NO can already react with atmospheric O_3 to form NO_2. In this study the plumes are measured shortly after their emission, while Berg et al. (2012) probably measured older plumes. Comparing the mean NO_x emission rate (11.0 ± 16.1 $g\,s^{-1}$) with the NO_2 emission rate of Berg et al. (2012) shows much better agreement between both. This is also supported by our calculated NO_2/NO_x ratio of 0.138, which indicates most NO_x is emitted as NO which then reacts with atmospheric ozone to form NO_2.

340   In general the result for a single measurement is prone to errors. The main reasons are due to the measurement geometry and the assumptions made in modelling the plume expansion. Only a small proportion of the light path is affected by the plumes of passing ships and as the LP-DOAS measures the integrated concentration along the light path, the measurement is influenced by the background variability along the light path. With a shorter light path, which only covers the main shipping lane and less background air masses, the enhancement in SO_2 and NO_2 would be more pronounced. This would increase the chances of

345   detecting the plume of a passing ship, even for ships with low emission rates.

      The main source of uncertainty is the plume modelling due to the uncertainty of the exact stack position and height and the simplification of turbulent structures within the plume. While the position of the ship's AIS receiver is known, the exact
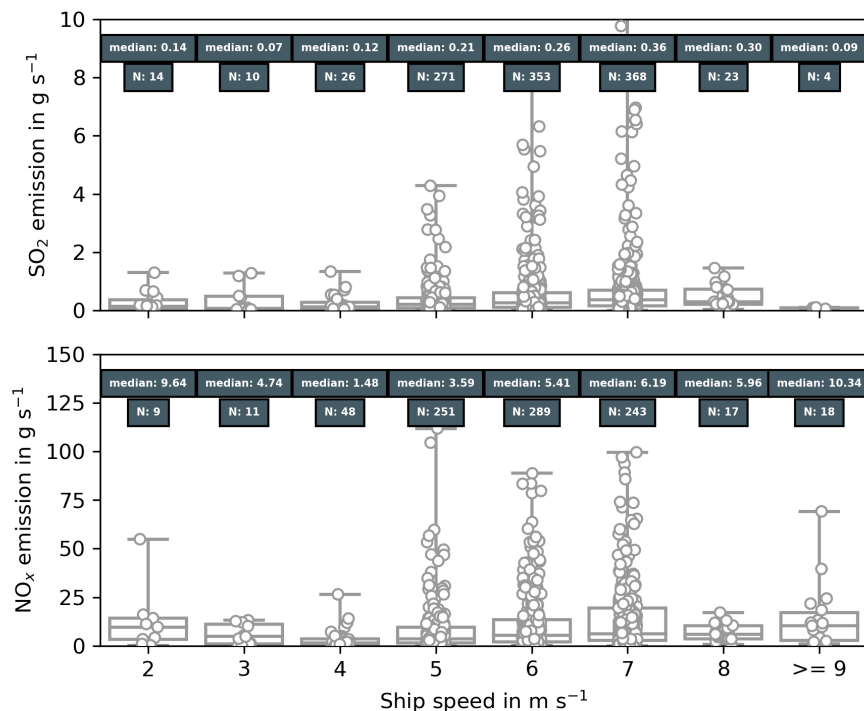
Figure 9. Box plot of SO$_2$ and NO$_x$ emission rates in g s^{-1} for different ship speeds. Boxes indicate the 25% and 75% percentile, the line in the middle is the median and the bars show minimum and maximum values. Dots show individual measurements. Boxes show the median emission rate and total number of observations for each ship speed.

position of the stack on the ship is unknown, which results in an uncertainty of the plume position and thus the modelled concentrations. A better knowledge of the exact position of the emission source would therefore increase the quality of the

350 derived emission rates and reduce the number of omitted emission rates.

However, repeated measurements of the same ship show a low variability in the derived emission rates with the exception of the dredging ships (e.g. Figure 6). The value of the calculated emission rates lies in the large number of measured ships and their statistics, which covers different meteorological conditions, and allows to characterize the emission behaviour of a fleet of ships entering the port of Hamburg.

355 **4   Summary and Conclusions**

A LP-DOAS instrument has been set up to measure ship emissions of SO$_2$ and NO$_2$ across the river Elbe, about 10 km seawards of Hamburg harbour. Between April 2018 and May 2019 a total number of 7402 passing ships have been identified and assigned to peaks in the trace gas time series. A method to derive ship emission rates of different trace gases was developed

Table 6. Comparison of emission rates derived from emission factors of other studies for two different fuel consumptions. Lower value is for a fuel consumption of $165\,\mathrm{kg\,h^{-1}}$, which is typical for inland ships. Upper value is for a fuel consumption of $2000\,\mathrm{kg\,h^{-1}}$ which is roughly the fuel consumption of a large container ship (14.000 TEU carrying capacity) at a speed of $7\,\mathrm{m\,s^{-1}}$ (Notteboom and Vernimmen, 2009).

Study	mean NO_x emission factor in $\mathrm{g\,kg^{-1}}$ fuel	NO_x emission rate in $\mathrm{g\,s^{-1}}$	number of evaluated ships
Moldanová et al. (2009)	73.4	3.4 - 40.8	1
Williams et al. (2009)	66.4 ± 9.1	3.0 - 36.9	> 200
Alföldy et al. (2013)	53.7 ± 22.3	2.5 - 29.8	497
Diesch et al. (2013)	53 ± 27	2.4 - 29.4	139
Beecken et al. (2014)	66.6 ± 23.4	3.1 - 37.0	174
Pirjola et al. (2014)	64.3 ± 24.6	2.9 - 35.7	11
Beecken et al. (2015)	58 ± 14.5	2.7 - 32.2	466
This study	-	mean 11.0	886
		median 4.6	
		mean seagoing 10.2	632
		median seagoing 5.2	
		mean inland 4.5	177
		median inland 1.9	

Table 7. Estimate of SO_2 emission rates for fuels with different fuel sulphur content, calculated for different fuel consumption under the assumption that all sulphur is converted to SO_2 during combustion. Lower value is for a fuel consumption of $165\,\mathrm{kg\,h^{-1}}$, which is typical for inland ships. Upper value is for a fuel consumption of $2000\,\mathrm{kg\,h^{-1}}$ which is roughly the fuel consumption of a large container ship at a speed of $6\,\mathrm{m\,s^{-1}}$ (Notteboom and Vernimmen, 2009), which is the typical speed for the largest passing vessels.

Source	Fuel type	Fuel sulphur content in % M/M	SO_2 emission rate in $\mathrm{g\,s^{-1}}$
Estimation	SECA limit	0.1	0.09 - 1.16
	Diesel fuel for inland shipping	1×10^{-5}	0.0009 - 0.0116
This study	-	-	mean 0.44
			median 0.25
			mean seagoing 0.47
			median seagoing 0.28
			mean inland 0.10
			median inland 0.05

and successfully applied to the measurements. The method uses a Gaussian plume model to simulate the plumes of passing ships and to derive the concentration the instrument would have measured given the assumptions made in the model. The calculated concentration is compared to the measured enhancement in the trace gas to calculate the emission rate. The derived emission rates have then to be filtered for non-physical results, which occur when the assumptions made for the model do not reflect the measurement situation. After filtering a total, of 886 NO_x, 1069 SO_2 and 1375 NO_2 emission rates were derived. The emission rates of inland and seagoing ships have been analysed and compared to each other and showed that sea going ships have higher emission rates than inland ships. Generally the emission rates increase with size and speed of the ship. The uncertainty for a single emission rate are 43 % in the mean and 35 % in median. Repeated measurements of several ships that passed multiple times show a low variability in their emission rates.

To improve the accuracy of the estimate of the ship emission rates, better knowledge of several key parameters will reduce their uncertainty. For example better knowledge of the exact position of the emission location i.e. the position of the ship's funnel, is required. Similarly, better knowledge of the height of the emission, i.e. the height of the funnel of the ship and the water level at the time of measurement, is required. The use of more sophisticated models to describe the shape and evolution of the plume would be of value. Additionally a measurement geometry with a shorter light path across the river would make it easier to detect the pollution plumes from water craft having small emissions and thereby increase the chances of determining emission rates from such vessels.

In comparison to the standard instrumentation at the measurement site, the LP-DOAS does not need to be calibrated and is able to measure under all wind conditions. However the current LP-DOAS system does not measure CO_2, so that relative emission factors cannot easily derived from NO_x/CO_2 or SO_2/CO_2 ratios. Therefore a model had to be used to calculate the emission rates of air pollutants. A measurement of the integrated CO_2 concentration along the light path would supersede the need for a dispersion model and should be considered for further technical developments of such measurements.

The measurements have demonstrated that accurate emission rates from shipping emissions can be derived from LP-DOAS measurements and that there is much potential in this approach. These emission rates are valuable input for the assessment of the influence of shipping emissions on air quality in regions close to the shipping lanes at the coast or along rivers and canals.

Author contributions. KK, SS and FW set up and operated the LP-DOAS instrument. AW provided the data of the in situ measurements. KK performed the analysis of the LP-DOAS data, provided the figures and wrote the manuscript. JB, DP, AR, SS, AW and FW supported the data interpretation. All authors contributed to the writing of the manuscript.

Competing interests. The authors declare that they have no conflict of interest.

Acknowledgements. The research project which facilitated the reported study was funded in part by the German Federal Maritime and Hydrographic Agency (Bundesamt für Seeschifffahrt und Hydrographie, BSH) and the University of Bremen. The authors thank the Waterways and Shipping Office Hamburg for their help and support.

References

Alföldy, B., Lööv, J. B., Lagler, F., Mellqvist, J., Berg, N., Beecken, J., Weststrate, H., Duyzer, J., Bencs, L., Horemans, B., Cavalli, F., Putaud, J.-P., Janssens-Maenhout, G., Csordás, A. P., van Grieken, R., Borowiak, A., and Hjorth, J.: Measurements of air pollution emission factors for marine transportation in SECA, Atmospheric Measurement Techniques, 6, 1777–1791, https://doi.org/10.5194/amt-6-1777-2013, 2013.

Balzani Lööv, J. M., Alfoldy, B., Gast, L. F. L., Hjorth, J., Lagler, F., Mellqvist, J., Beecken, J., Berg, N., Duyzer, J., Westrate, H., Swart, D. P. J., Berkhout, A. J. C., Jalkanen, J.-P., Prata, A. J., van der Hoff, G. R., and Borowiak, A.: Field test of available methods to measure remotely SO x and NO x emissions from ships, Atmospheric Measurement Techniques, 7, 2597–2613, https://doi.org/10.5194/amt-7-2597-2014, 2014.

Beecken, J., Mellqvist, J., Salo, K., Ekholm, J., and Jalkanen, J.-P.: Airborne emission measurements of SO_2, NO_x and particles from individual ships using a sniffer technique, Atmospheric Measurement Techniques, 7, 1957–1968, https://doi.org/10.5194/amt-7-1957-2014, 2014.

Beecken, J., Mellqvist, J., Salo, K., Ekholm, J., Jalkanen, J.-P., Johansson, L., Litvinenko, V., Volodin, K., and Frank-Kamenetsky, D. A.: Emission factors of SO_2, NO_x and particles from ships in Neva Bay from ground-based and helicopter-borne measurements and AIS-based modeling, Atmospheric Chemistry and Physics, 15, 5229–5241, https://doi.org/10.5194/acp-15-5229-2015, 2015.

Berg, N., Mellqvist, J., Jalkanen, J.-P., and Balzani, J.: Ship emissions of SO_2 and NO_2: DOAS measurements from airborne platforms, Atmospheric Measurement Techniques, 5, 1085–1098, https://doi.org/10.5194/amt-5-1085-2012, 2012.

Briggs, G. A.: Diffusion estimation for small emissions. Preliminary report, https://doi.org/10.2172/5118833, 1973.

Cheng, Y., Wang, S., Zhu, J., Guo, Y., Zhang, R., Liu, Y., Zhang, Y., Yu, Q., Ma, W., and Zhou, B.: Surveillance of SO_2 and NO_2 from ship emissions by MAX-DOAS measurements and the implications regarding fuel sulfur content compliance, Atmospheric Chemistry and Physics, 19, 13 611–13 626, https://doi.org/10.5194/acp-19-13611-2019, 2019.

Clapp, L.: Analysis of the relationship between ambient levels of O3, NO2 and NO as a function of NOx in the UK, Atmospheric Environment, 35, 6391–6405, https://doi.org/10.1016/S1352-2310(01)00378-8, 2001.

Cooper, D.: Exhaust emissions from high speed passenger ferries, Atmospheric Environment, 35, 4189–4200, https://doi.org/10.1016/S1352-2310(01)00192-3, 2001.

Diesch, J.-M., Drewnick, F., Klimach, T., and Borrmann, S.: Investigation of gaseous and particulate emissions from various marine vessel types measured on the banks of the Elbe in Northern Germany, Atmospheric Chemistry and Physics, 13, 3603–3618, https://doi.org/10.5194/acp-13-3603-2013, 2013.

DWD Climate Data Center: Historical 10-minute station observations of solar incoming radiation,longwave downward radiation and sunshine duration for Germany, version V1, a.

DWD Climate Data Center: Selected 81 stations, distributed over Germany, in the traditional KL-standard format, version recent, b.

Eyring, V.: Emissions from international shipping: 1. The last 50 years, Journal of Geophysical Research, 110, https://doi.org/10.1029/2004JD005619, 2005.

Eyring, V., Isaksen, I. S., Berntsen, T., Collins, W. J., Corbett, J. J., Endresen, O., Grainger, R. G., Moldanova, J., Schlager, H., and Stevenson, D. S.: Transport impacts on atmosphere and climate: Shipping, Atmospheric Environment, 44, 4735–4771, https://doi.org/10.1016/j.atmosenv.2009.04.059, 2010.

Kattner, L.: Measurements of shipping emissions with in-situ instruments, Dissertation, Universität Bremen, Bremen, 2019.

Kattner, L., Mathieu-Üffing, B., Burrows, J. P., Richter, A., Schmolke, S., Seyler, A., and Wittrock, F.: Monitoring compliance with sulfur content regulations of shipping fuel by in situ measurements of ship emissions, Atmospheric Chemistry and Physics, 15, 10 087–10 092, https://doi.org/10.5194/acp-15-10087-2015, 2015.

430 Kurtenbach, R., Vaupel, K., Kleffmann, J., Klenk, U., Schmidt, E., and Wiesen, P.: Emissions of NO, NO 2 and PM from inland shipping, Atmospheric Chemistry and Physics, 16, 14 285–14 295, https://doi.org/10.5194/acp-16-14285-2016, 2016.

MarineTraffic: MarineTraffic – Global Ship Tracking Intelligence (www.marinetraffic.com), https://www.marinetraffic.com/.

Meller, R. and Moortgat, G. K.: Temperature dependence of the absorption cross sections of formaldehyde between 223 and 323 K in the wavelength range 225-375 nm, Journal of Geophysical Research, 105, 7089–7101, https://doi.org/10.1029/1999JD901074, 2000.

435 Moldanová, J., Fridell, E., Popovicheva, O., Demirdjian, B., Tishkova, V., Faccinetto, A., and Focsa, C.: Characterisation of particulate matter and gaseous emissions from a large ship diesel engine, Atmospheric Environment, 43, 2632–2641, https://doi.org/10.1016/j.atmosenv.2009.02.008, 2009.

Notteboom, T. E. and Vernimmen, B.: The effect of high fuel costs on liner service configuration in container shipping, Journal of Transport Geography, 17, 325–337, https://doi.org/10.1016/j.jtrangeo.2008.05.003, 2009.

440 Pasquill, F.: Atmospheric diffusion: The dispersion of windborne material from industrial and other sources, 1. publ., reprint edn., 1968.

Pirjola, L., Pajunoja, A., Walden, J., Jalkanen, J.-P., Rönkkö, T., Kousa, A., and Koskentalo, T.: Mobile measurements of ship emissions in two harbour areas in Finland, Atmospheric Measurement Techniques, 7, 149–161, https://doi.org/10.5194/amt-7-149-2014, 2014.

Ramacher, M. O. P., Karl, M., Aulinger, A., Bieser, J., Matthias, V., and Quante, M.: The Impact of Emissions from Ships in Ports on Regional and Urban Scale Air Quality, in: Air Pollution Modeling and its Application XXV, edited by Mensink, C. and Kallos, G.,

445 Springer Proceedings in Complexity, pp. 309–316, Springer International Publishing, Cham, https://doi.org/10.1007/978-3-319-57645-9_49, 2018.

Ramacher, M. O. P., Matthias, V., Aulinger, A., Quante, M., Bieser, J., and Karl, M.: Contributions of traffic and shipping emissions to city-scale NOx and PM2.5 exposure in Hamburg, Atmospheric Environment, 237, 117 674, https://doi.org/10.1016/j.atmosenv.2020.117674, 2020.

450 Serdyuchenko, A., Gorshelev, V., Weber, M., Chehade, W., and Burrows, J. P.: High spectral resolution ozone absorption cross-sections – Part 2: Temperature dependence, Atmospheric Measurement Techniques, 7, 625–636, https://doi.org/10.5194/amt-7-625-2014, 2014.

Seyler, A., Wittrock, F., Kattner, L., Mathieu-Üffing, B., Peters, E., Richter, A., Schmolke, S., and Burrows, J. P.: Monitoring shipping emissions in the German Bight using MAX-DOAS measurements, Atmospheric Chemistry and Physics, 17, 10 997–11 023, https://doi.org/10.5194/acp-17-10997-2017, 2017.

455 Seyler, A., Meier, A. C., Wittrock, F., Kattner, L., Mathieu-Üffing, B., Peters, E., Richter, A., Ruhtz, T., Schönhardt, A., Schmolke, S., and Burrows, J. P.: Studies of the horizontal inhomogeneities in NO$_2$concentrations above a shipping lane using ground-based multi-axis differential optical absorption spectroscopy (MAX-DOAS) measurements and validation with airborne imaging DOAS measurements, Atmospheric Measurement Techniques, 12, 5959–5977, https://doi.org/10.5194/amt-12-5959-2019, 2019.

Stutz, J. and Platt, U.: Numerical analysis and estimation of the statistical error of differential optical absorption spectroscopy measurements

460 with least-squares methods, Applied optics, 35, 6041–6053, https://doi.org/10.1364/ao.35.006041, 1996.

Stutz, J., Kim, E. S., Platt, U., Bruno, P., Perrino, C., and Febo, A.: UV-visible absorption cross sections of nitrous acid, Journal of Geophysical Research, 105, 14 585–14 592, https://doi.org/10.1029/2000JD900003, 2000.

Tang, L., Ramacher, M. O. P., Moldanová, J., Matthias, V., Karl, M., Johansson, L., Jalkanen, J.-P., Yaramenka, K., Aulinger, A., and Gustafsson, M.: The impact of ship emissions on air quality and human health in the Gothenburg area – Part 1: 2012 emissions, Atmospheric

465   Chemistry and Physics, 20, 7509–7530, https://doi.org/10.5194/acp-20-7509-2020, 2020.

Thalman, R. and Volkamer, R.: Temperature dependent absorption cross-sections of O2-O2 collision pairs between 340 and 630 nm and at atmospherically relevant pressure, Physical chemistry chemical physics : PCCP, 15, 15 371–15 381, https://doi.org/10.1039/c3cp50968k, 2013.

Vandaele, A. C., Hermans, C., Simon, P. C., van Roozendael, M., Guilmot, J. M., Carleer, M., and Colin, R.: Fourier transform mea-

470   surement of NO2 absorption cross-section in the visible range at room temperature, Journal of Atmospheric Chemistry, 25, 289–305, https://doi.org/10.1007/BF00053797, 1996.

Williams, E. J., Lerner, B. M., Murphy, P. C., Herndon, S. C., and Zahniser, M. S.: Emissions of NO x , SO 2 , CO, and HCHO from commercial marine shipping during Texas Air Quality Study (TexAQS) 2006, Journal of Geophysical Research, 114, https://doi.org/10.1029/2009JD012094, 2009.